communications earth & environment

Article

A Nature Portfolio journal

Article in Press

https://doi.org/10.1038/s43247-026-04041-6

Holocene summer and winter temperature trends and excursions in East-Central Europe from Carpathian pollen records

Check for updates

Jon Camuera [1] ✉, Enikő K. Magyari [2,3] ✉, János L. Korponai [4,5], Niina Kuosmanen[6], Lu Chenao[6], Abigail A. Ofosu-Brakoh [2], Yuanhao Xu[7] & Heikki Seppä [6]

This study reconstructs summer and winter temperatures for East-Central Europe (ECE) over the last 12 ka using pollen records from five mid-altitude sites in the Carpathian Mountains. Seasonal reconstructions were combined into composite records and statistically evaluated to identify significant long-term trends and short-term excursions. Both seasons reveal strong Early Holocene warming, followed by contrasting trajectories. Summer temperatures peaked at 7.2 ka (1.4 °C above Holocene mean) and then gradual declined, whereas winter temperatures continued rising until a Late Holocene maximum at 2.1 ka (1.7 °C above Holocene mean) before decreasing during the last two millennia. These opposing trends indicate a progressive reduction in continentality across ECE over the last 6 ka. The 8.2 ka event represents the only statistically significant short-term excursion, with a cooling of 2 °C in summer and 2.4 °C in winter. Comparison with independent proxy records and climate model simulations shows broad agreement with reconstructed pattern of Holocene seasonal temperature evolution.

Although the Holocene is one of the most extensively studied periods of the Quaternary, substantial debate persists regarding temperature trends over the past 12 ka, particularly when evaluated on a quantitative scale. Key uncertainties include potential seasonal biases[1–3], the quality of available proxy datasets used[4], proxy-specific reconstruction biases[5–8], and the definition and reliable detection of abrupt temperature or precipitation excursions[9–11]. These questions add uncertainty to the Holocene proxy-model comparisons and climate model validations[3,12] and underscore the importance of rigorous standards in the proxy datasets used to quantify past climatic changes.

In Holocene climate studies, pollen-based climate reconstructions are in the core of this debate because pollen data are the most common type of data in the global Temperature 12 k database[13]. There are many requirements for the reliable use of pollen data in climate reconstructions, such as availability of organic sediment cores and limited prehistoric human impact on vegetation[14,15]. One important but often overlooked question is the location of the sites from where the fossil biological data is collected. Fossil pollen sites situated in the middle of large biomes with nearly uniform vegetation composition require large climatic changes to produce detectable shifts in vegetation[16]. In contrast, sites situated in pronounced climatic and ecological transition zones are much more sensitive to climatic variation. When vegetation at these sites is controlled by just one or two dominant climatic variables, even modest changes in those variables can lead to strong variability in vegetation and pollen composition.

In Eastern Central Europe (ECE), these requirements for climatic sensitivity are best met in the Carpathian Mountains. The Carpathians are predominantly forested with deciduous and coniferous species, with composition varying by altitude, slope and local climatic conditions[17]. The region contains Europe's largest remaining tracts of primeval beech forest[18], many of which retain near-natural species assemblages[19]. A wide range of biological proxies has been applied to produce quantitative climate reconstructions in the Carpathians. These include biotic indicators such pollen[20] chironomids[21–24], diatoms[25], testate amoebae (Ruskál et al., 2020; Schnitchen et al., 2006), tree rings[26,27] and biomarkers[28]. Non-biotic proxies have also been used, including inorganic geochemistry, magnetic susceptibility and stable isotopes from lake sediments and speleothems[29–33]. Despite this

[1]Andalusian Earth Sciences Institute (IACT), Spanish National Research Council (CSIC), Armilla, Granada, Spain. [2]Institute of Geography and Earth Sciences, Department of Environmental and Landscape Geography, Eötvös Loránd University, Budapest, Hungary. [3]HUN-REN-MTM-ELTE Research group for Paleontology, Budapest, Hungary. [4]Department of Aquatic Environmental Sciences, Faculty of Water Sciences, Ludovika University of Public Service, Budapest, Hungary. [5]Department of Environmental Science, Sapientia Hungarian University of Transylvania, Cluj-Napoca, Romania. [6]Department of Geosciences and Geography, Faculty of Science, University of Helsinki, Helsinki, Finland. [7]School of Civil Engineering, Sun Yat-sen University, Guangzhou, China. ✉e-mail: jon.camuera@csic.es; eniko.magyari@ttk.elte.hu

extensive research, there is still no consensus on the trends and magnitude of the Holocene summer and winter temperatures. Moreover, small-scale regional variations on decadal to centennial timescales, associated with rapid and abrupt temperature excursions, have not yet been verified through detailed statistical analyses.

To address these questions, we use pollen data to reconstruct summer and winter temperatures in ECE. Specifically, we select fossil pollen records from five sites in the Carpathians (Fig. 1) where vegetation dynamics have been strongly influenced by seasonal temperature changes[34]. Using a regionally designed pollen-climate calibration model, we generate quantitative reconstructions of summer and winter temperatures for each site. These individual records are combined into composite series, providing high-resolution reconstructions of seasonal temperature variability across ECE. In addition, we also assess the statistical significance of both long-term trends and short-term excursions in the composites under the Scale-Normalized SIgnificant ZERo crossing of derivatives (SnSiZer) analysis. The objectives of this study are: (1) to generate decadal-resolution, pollen-based quantitative reconstructions of summer and winter temperatures for the Carpathian region, with the aim of improving knowledge of Holocene short- and long-term temperature variability in mid-altitude areas of ECE, supported by robust statistical analyses, (2) to compare our seasonal temperature reconstructions with other regional quantitative paleoclimate records, and (3) to identify the main drivers of the summer and winter temperature trends.

Results

The composite of the main pollen taxa from the five fossil records shows the supraregional vegetation changes in the Carpathian region over the last 12,000 years (Fig. S1). The individual quantitative reconstructions from these records suggest similar summer and winter temperature trends throughout the Holocene, with raw values ranging between ca. 14 and 19 °C for summer, and between ca. −5 and 2 °C for winter (Fig. S2). Throughout the text and figures, temperature changes are presented as deviations from the Holocene mean (Figs. 2–5). In some cases, temperatures are also compared with modern values. Modern temperatures were calculated as the mean of the reconstructed values over the last 200 years. The modern summer temperature is 1 °C below Holocene mean, whereas the modern winter temperature is 0.2 °C above the Holocene mean (yellow stars in Fig. 2).

Statistically significant summer and winter temperature trends

From the beginning of the record until 9.9 ka, the summer temperature shows a statistically significant Early Holocene increase of 1 °C. This warming culminates in a prolonged interval of elevated summer temperatures, peaking at 7.2 ka with 1.4 °C higher than the Holocene mean (2.4 °C above present), and persisting until 6.1 ka. After 6.1 ka, the summer temperatures declined by 1.9 °C until 1.1 ka, and over the last 1.1 ka they remained relatively stable (Fig. 3).

Winter temperatures at 12 ka were 2.2 °C lower than present and increased 2.1 °C during the Early Holocene (from 12 to 9.2 ka). Winter temperatures increased gradually from 7.8 to 2.6 ka by 1.7 °C. This warming trend culminated at 2.1 ka, when winters were 1.7 °C warmer than the Holocene mean and 1.5 °C warmer than today, and represents the warmest winter conditions in ECE. It was followed by a statistically significant cooling trend, with winter temperatures decreasing by 0.7 °C between 1.7 and 0.4 ka (Fig. 4).

The summer thermal maximum at 7.2 ka contrasts with the winter temperature maximum at 2.1 ka, showing distinct seasonal trends. Temperatures increased in both seasons during the Early Holocene, but they begin to diverge during the Mid Holocene. Over the last ca. 6 ka, the opposing trends in summer and winter temperatures indicate a progressive reduction in continentality and an increase in oceanic influence in ECE during the Late Holocene.

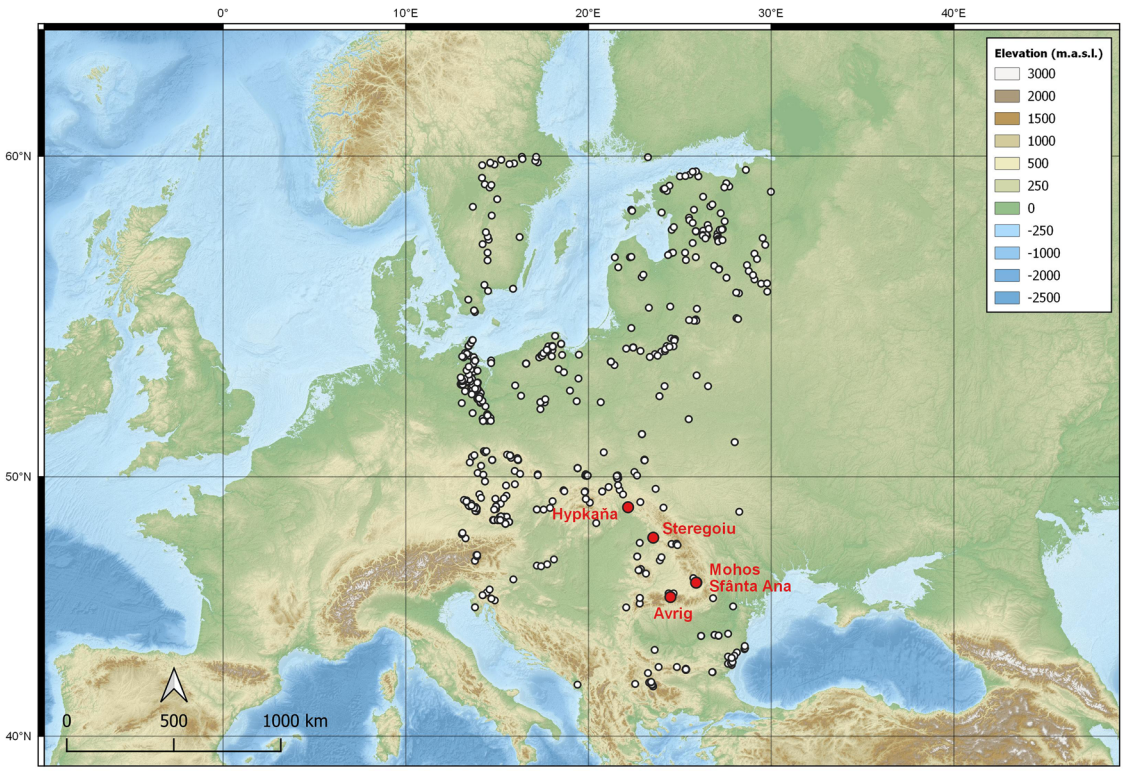

Fig. 1 | Location of the fossil pollen records (red dots) from the Carpathian Mountains used for the quantitative temperature reconstructions. White dots represent the modern pollen calibration set used in this study.

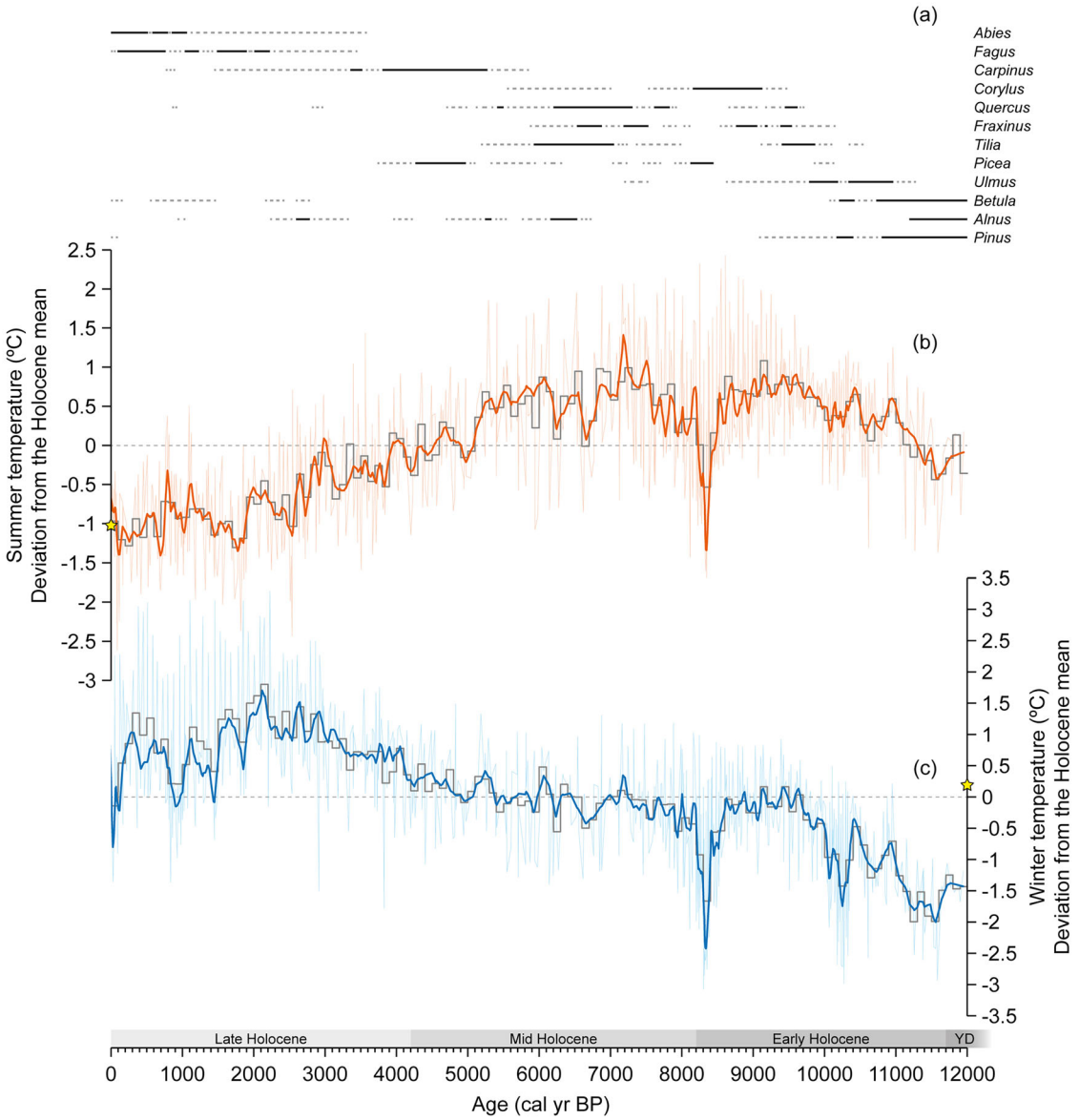

Fig. 2 | Composite regional summer and winter temperature reconstruction (°C) from the Carpathians. a Occurrence of main tree taxa based on the composite of the five Carpathian fossil pollen records used (see Figs. S7–S11). Grey dashes lines indicate periods with abundance values above the 70th percentile and black lines above the 90th percentile for each taxon, based on Fig. S1. **b**, **c** Orange and blue lines represent the mean summer and winter temperatures deviations from the Holocene mean, respectively. Light lines indicate the raw reconstructed data, dark lines correspond to the LOESS smoothing of 0.015 and grey lines the average values at 100-year intervals. Yellow stars represent the modern temperature values, calculated as the mean of the last 200 years.

Summer and winter temperature excursions

The strongest and most abrupt statistically relevant temperature excursions in both summer and winter temperatures were recorded during the 8.2 ka event. This temperature decline is primarily driven by the expansion of *Picea*, a taxon with low summer and winter temperature optima (Fig. S3), together with the decline of thermophilous taxa such as *Tilia*, *Fraxinus* and *Quercus*. In summer, the temperature dropped 2 °C over 190 years (8.53–8.34 ka), indicating a cooling rate of 1.05 °C per century. This cooling was followed by a recovery, with temperatures increasing by 2.1 °C over 150 years (8.34–8.19 ka), corresponding to an average warming of 1.4 °C per century. For winter temperatures, a decrease of 2.4 °C occurred over 290 years (8.63–8.34 ka), reflecting a cooling of 0.83 °C per century. This cooling phase was followed by a recovery of 2.3 °C over 150 years (8.34–8.19 ka), suggesting a warming rate of 1.53 °C per century (Figs. 2–4).

Additionally, both summer and winter reconstructions show several statistically non-significant climate excursions, with the summer and winter temperature drops of 0.5–1.4 °C at 10.4–10.2 ka as the most representative ones (Figs. 2–4).

Discussion

Potential non-climatic drivers of vegetation change

It is necessary to note that other factors than climate, such human impact, can influence the current and Holocene distribution and abundance patterns of vegetation. Pollen records across the Carpathian lowlands show that human impact is present since around 8 ka BP[35,36], but the first clearly larger, landscape-scale clearances are visible after 5 ka and particularly from the Late Bronze Age onward (after ca. 3.6 ka BP) when many lowland areas were transformed into cultural steppe[36,37]. By contrast, in the high Carpathians, anthropogenic signals generally appeared later and were weaker. In the Carpathians, the first signals are dated to about 3 ka BP, with stronger and more sustained human impact from 2 to 1.5 ka onward[38,39], while in the East Carpathians clear anthropogenic opening, grazing indicators and treeline lowering strengthened during the Late Holocene, especially from roughly

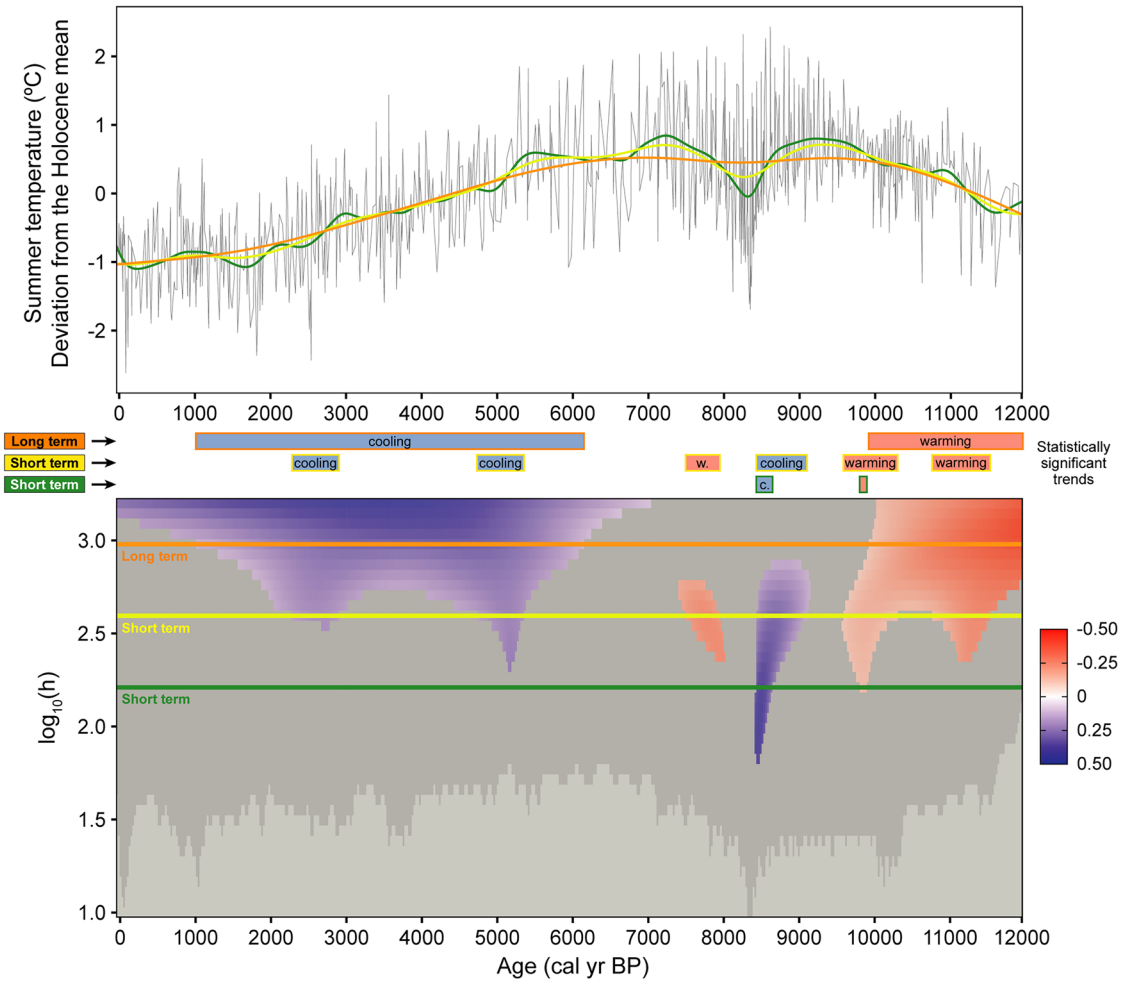

Fig. 3 | SnSiZer analysis run on the composite summer temperature reconstruction. The top panel shows the raw summer reconstruction data (deviation from the Holocene mean). The bottom panel represents the SnSiZer results, with red and blue clouds (reading from past to present) indicating the statistically significant increasing and decreasing temperatures. The green, yellow and orange lines (in both panels) represent the three smoothing levels. Dark grey areas represent non-significant changes, whereas light grey areas represent low sampling resolution.

the Late Bronze Age (3.6 ka BP) onward and intensified in the Iron Age/Medieval period[40,41].

Tree-species ranges and abundances were likely shaped not only by climate, but also by disturbance regimes, migration history and interspecific competition. These processes are important for pollen-based climate reconstruction because changes in pollen abundance may reflect ecological processes that are not directly proportional to regional temperature change. During the Early Holocene, the thermophilous broadleaf taxa, including *Ulmus*, *Tilia*, *Fraxinus*, and *Quercus*, expanded together with *Corylus*, while *Pinus*, *Betula*, and *Alnus* gradually declined. The prolonged dominance of *Corylus* in the Carpathian colline and lower montane belt (Figs. 2a and S1) is therefore a defining feature of Early Holocene pollen assemblages[42]. This dominance likely reflects the high pollen productivity of *Corylus* and its competitive advantage under relatively open or disturbed forest conditions.

Its expansion in the Carpathians between ca. 10.5 and 9.5 ka (Figs. 2a and S1) was probably promoted by favorable climate conditions, but also by frequent fires[38,43]. Fire should not be regarded as entirely independent of climate, because increased burning may have been favored by warmer and/or drier seasonal conditions. However, fire affects vegetation through disturbance-mediated pathways, and therefore *Corylus* expansion may partly represent an indirect ecological response rather than a direct temperature signal. Under these conditions, *Corylus* outcompeted *Ulmus* and locally *Quercus*, consistent with its high drought tolerance and broad thermal niche[44–46]. Its Mid Holocene decline is also best interpreted as a shift in interspecific competitive balance rather than simple climatic exclusion. Around 5.5 ka, *Carpinus betulus* expanded at many mid-altitude sites and progressively replaced *Corylus* (Figs. 2a and S1), despite partly overlapping climatic tolerances. In the eastern and southern Carpathians, this led to a distinct *Carpinus* phase that preceded the major spread of *Fagus sylvatica*. *Fagus* is a strong ecological competitor because of its shade tolerance and capability to form dense canopies, allowing it to outcompete less shade-tolerant taxa and to form monospecific late successional forests. Such competitive replacement can dampen or delay the pollen response to climate change, because changes in forest composition may partly reflect successional dynamics rather than direct temperature forcing.

Regarding the Late Holocene, regional tree-population dynamics in the Carpathians indicate an expansion of *Alnus* and *Betula* between 1.5 and 1 ka (Fig. S1). In the calibration model these taxa show low winter temperature optima (Fig. S3), therefore their increases contribute to cooler reconstructed winter temperatures. These taxa are characteristic of early-successional stages that often expand following forest clearance, land abandonment or drying mire surfaces[47]. In agreement with the generally increasing anthropogenic deforestation events in the Carpathians mentioned above, the increases of *Alnus* and *Betula* can be attributed to secondary forest succession and local establishment on the drying mire surfaces[47–49]. This suggest that their Late Holocene increase should not be interpreted solely as evidence for regional winter cooling. Instead, it may partly reflect secondary

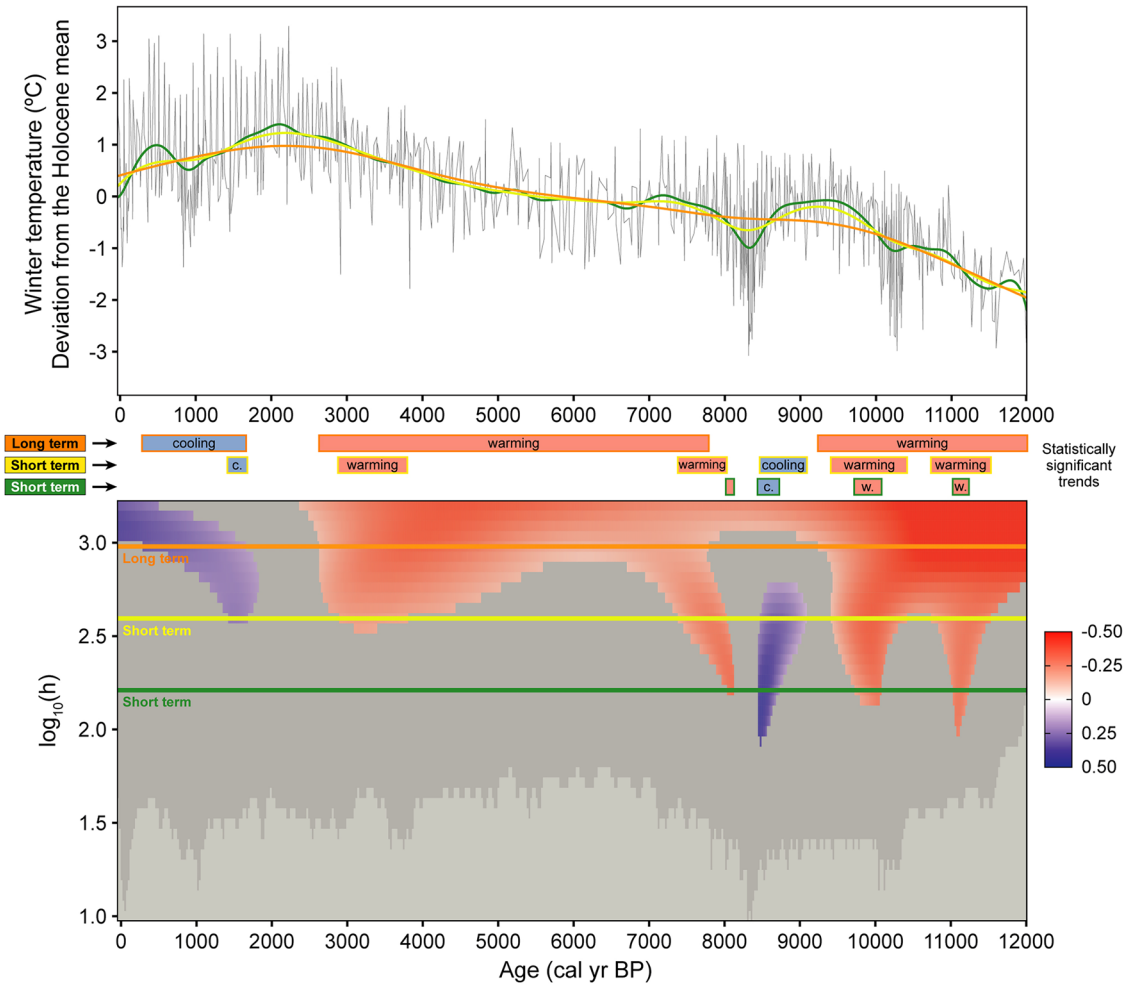

Fig. 4 | Same as Fig. 3 but for the composite winter temperature reconstruction.

succession and local hydroseral development, which could bias the pollen-based reconstruction toward lower winter-temperature estimates.

Summer temperature trend

Our summer temperature reconstruction reveals a clear and statistically significant sequence of Holocene climate phases, characterized by an increasing trend between 12 and 9.5 ka, a summer temperature maximum from 9.5 to 5.5 ka and a subsequent cooling toward the present. These patterns can be compared with the pollen-based climate reconstructions of Feurdean et al. (2008), who used the same fossil pollen site from Steregoiu as in our study. In Feurdean et al. (2008), their mean temperature of the warmest month (MTWA) exhibit relatively stable temperatures from 11.5 to 4.5 ka, followed by an increase between 4.5 and 2.5 ka, and a decline over the last 2.5 ka. Although our Steregoiu record also shows a temperature decrease at 7–6 ka, mainly associated with the expansion of *Picea* and a decline in *Ulmus* abundance (Fig. S2), the overall trend of our composite record is nearly opposite to that reported by Feurdean et al. (2008), except during the last 2.5 ka.

A further comparison with pollen-based climate reconstructions from the Carpathians by Cruz-Silva et al. (2023) shows that their summer temperature reconstructions (MTWA) from Steregoiu, Mohos and Avrig indicate the lowest values during the Early and Mid Holocene (until 6–5 ka), followed by a rapid warming between approximately 6 to 4 ka (Fig. S4). This pattern contrasts with both our summer temperature reconstructions from the same sites and the Carpathian composite record (Figs. 2 and S4). These discrepancies in Holocene summer temperature trends, despite being based on the same fossil pollen datasets, likely reflect differences in the calibration datasets used. The pronounced rise in reconstructed summer temperatures from 6 to 4 ka in Cruz-Silva et al. (2023) suggests that *Carpinus* and *Fagus* are considered as indicators of high summer temperature in their pollen-climate calibration model, whereas our tolerance spectra clearly show that *Carpinus* does not exhibit the highest summer temperature optimum among the tree taxa and *Fagus* is characterized by one of the lowest temperature optima (Fig. S3).

To further evaluate our reconstruction and assess the differences in the pollen-based reconstructions, we compare the composite record with other proxy-based reconstructions, including chironomid-inferred July temperatures from Lake Brazi in the southern Carpathians[21] (Fig. 5c). Although the absolute temperature values differ, the Brazi record exhibits the same overall structure, with a rapid Early Holocene warming, a period of maximum summer temperatures, and a Mid to Late Holocene decline, closely matching our composite record (Fig. 5d). The main difference is that the Mid Holocene thermal maximum at Brazi ends at 6.7 ka, approximately 500 years later than in our composite.

We also compare the ECE composite[50] with summer temperature simulations from the CHELSA-TraCE-21k model[51]. This model is based on the TraCE-21ka simulation performed with the CCSM3 climate model[52] and provides high-resolution (30-arcsec, 100-year time steps) downscaled temperature fields (Fig. 5b). The comparison shows broad agreement between reconstructed and simulated summer temperatures, including the interval of elevated temperatures and the gradual cooling over the last 6 ka. The simulation suggests Holocene summer temperatures range of 4 °C (17.5–21.5 °C), whereas our reconstruction indicates a narrower range of 3 °C between the minimum and maximum values (Fig. 2). The simulated

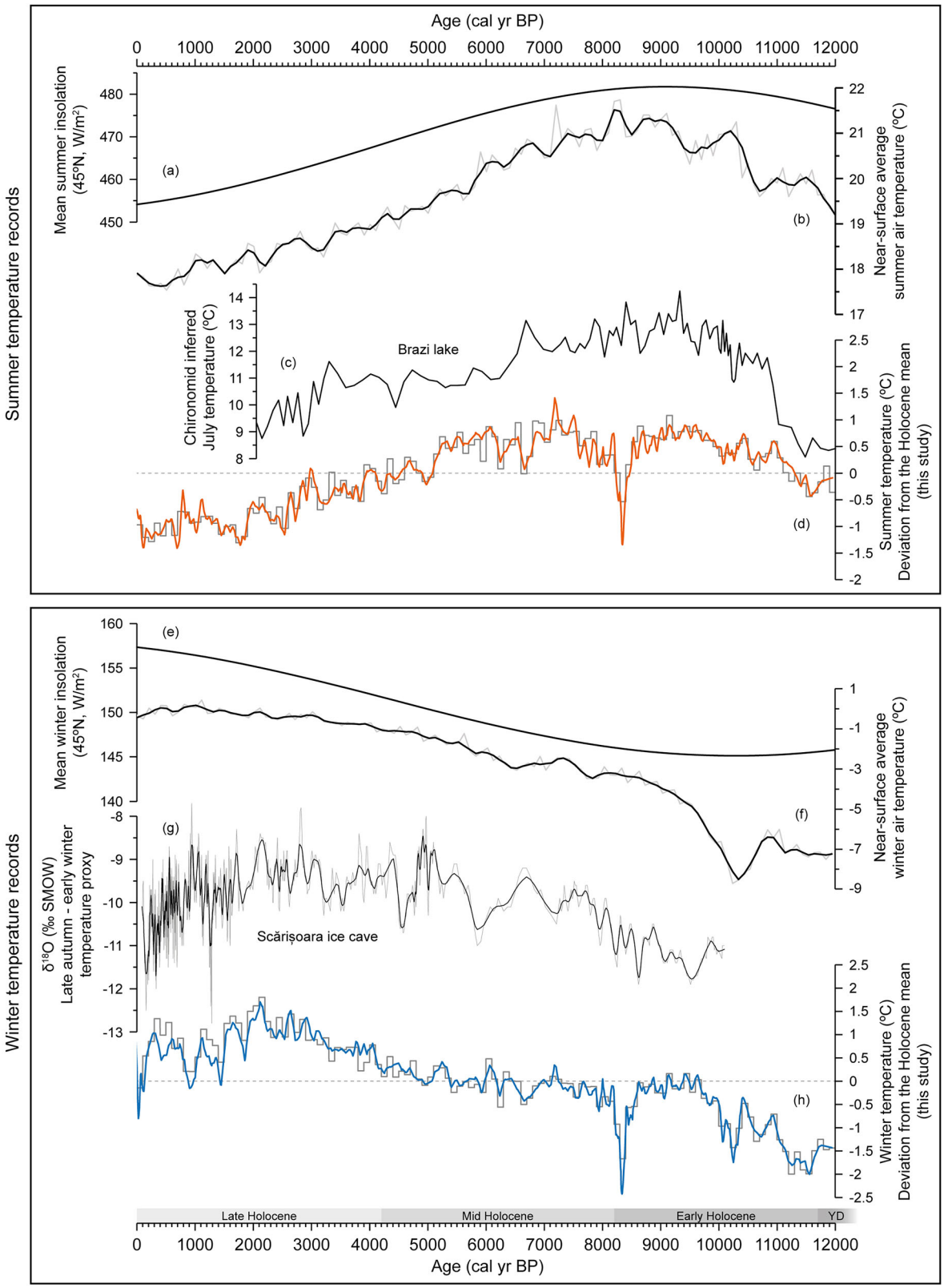

Fig. 5 | Compilation of regional summer and winter temperature records. The top panel shows summer temperatures records, including: **a** mean summer (JJA, 1 June–31 August) insolation at 45°N[90], **b** near-surface average summer air temperatures simulation (CHELSA-TraCE21k model)[51], **c** chironomid inferred July temperature from Brazi lake (Romanian Carpathians)[21], and **d** Carpathian summer temperature reconstruction, deviation from the Holocene mean (this study). The bottom panel shows winter temperature records, including: **e** mean winter (DJF, 1 December–28 February) insolation at 45°N[90], **f** near-surface average summer air temperatures simulation (CHELSA-TraCE21k model)[51], **g** autumn-winter temperature from Scărișoara ice cave (Romanian Carpathians)[29], and **h** Carpathian winter temperature reconstruction, deviation from the Holocene mean (this study). In the Carpathian reconstructions (**d** and **h**), orange and blue lines correspond to the LOESS smoothing (0.015) and grey lines to the average values at 100-year intervals.

temperatures are strongly driven by summer insolation, a relationship also evident in our composite record (Fig. 5a and d).

Winter temperature trend

The ECE winter temperature composite diverges from the summer record, showing a progressive increase of 3.7 °C from Early to Late Holocene (11.5–2.1 ka), followed by a cooling of 2.1 °C during the last 2.1 ka (Figs. 2, 4, and 5h). A previous reconstruction of the mean temperature of the coldest month (MTCO)[20], identified peak values between 9.5 and 8.5 ka and again during the last 2.5 ka, with a cooler interval in the Mid Holocene. The MTCO reconstruction of Cruz-Silva et al. (2023) shows an Early and Mid Holocene temperature evolution broadly consistent with our composite winter record (Fig. S5).

To further validate the reconstructions, we compare the ECE winter temperature composite with additional temperature-sensitive proxy records from the region, including the $\delta^{18}O$ record from Scărișoara ice cave[29]. This archive is interpreted to reflect late-autumn to early-winter temperatures and is therefore well suited for comparison with the ECE winter reconstruction. Both records indicate rising temperatures during the Early and Mid Holocene. The Scărișoara $\delta^{18}O$ peak at 5 ka and remain relatively stable until a decline over the last 1 ka, diverging from the continued increase in the ECE composite until 2.1 ka (Fig. 5g, h). The $\delta^{18}O$-based winter temperature reconstruction from Urșilor cave (Romanian Carpathians) shows even closer agreement with the ECE composite, exhibiting an increasing trend through the Mid and Late Holocene (6–1 ka) followed by cooling during the last millennium[53]. Overall, although the winter temperature trends inferred from pollen and cave $\delta^{18}O$ records are not identical, they are broadly consistent. Together, these independent proxies support the general pattern of the ECE winter temperature composite and reinforce the credibility of this long-term evolution.

In the CHELSA-TraCE-21k simulation, although the model does not capture small-scale winter oscillations (Fig. 5f), it shows the overall winter temperature trends observed in our reconstruction. In the model, winter temperature rises rapidly by 3 to 4 °C from 12 to 10.5 to 9 ka, followed by a slower and more gradual rise of 4 °C throughout the rest of the Holocene (from 9 ka to present). This long-term trend broadly aligns with the 2.2 °C increase reconstructed in the ECE winter temperature composite between 10 and 2 ka. As with the summer record, both proxy-based reconstructions and model simulations suggest that winter temperatures in ECE were likely influenced by winter insolation (Fig. 5e and h). A notable discrepancy between the reconstruction and the insolation curve is the pronounced peak at 2.1 ka and the subsequent temperature decline toward the present in the composite, an evolution that is not reproduced by the model. Determining whether this Late Holocene winter cooling represents a robust regional signal will require additional records from sites less affected by confounding factors such as human impact.

Short-term cold excursions

The only statistically significant short-term excursion in both summer and winter temperature trends is the cooling event between 8.6 and 8.2 ka, characterized by decreases of 2 °C in summer and 2.4 °C in winter (Figs. 2–4). This cold excursion (8.6–8.2 ka) most likely corresponds to the 8.2 ka cold event[54,55], generally attributed to a disruption of the Atlantic Meridional Overturning Circulation (AMOC) triggered by large freshwater inputs following the sudden drainage of ice-dammed lakes or the collapse of the Laurentide Ice Sheet[56,57].

Although the 8.2 ka event is widely documented across Europe and the Mediterranean[10], evidence from ECE has been less consistent. Pollen-based reconstructions from Steregoiu by Feurdean et al. (2008) indicate a winter cooling of 4–5 °C, while summer temperature shows an unexpected increase during the event. The reconstruction by Cruz-Silva et al. (2023) indicates a summer temperature decrease of 3 °C at Steregoiu, consistent with our results (Fig. S4), whereas their data suggest a winter cooling of 7 °C, substantially larger than the 3 °C decrease identified in our study (Fig. S5).

However, part of the reconstructed cooling may have been amplified by local vegetation succession associated with the infilling of the shallow lake during the 8.2 ka event, when the expansion of *Filipendula ulmaria* with low temperature optima in the modern calibration dataset likely biased the pollen-based reconstruction towards cooler temperatures. This signal is predominantly driven by changes in pollen composition at Steregoiu, which provides high-resolution data around the 8.2 ka event (Fig. S8)[20]. This former crater lake transitioned from a lake into an open fen and carr ecosystem between 8.6 and 8.2 ka, culminating in the local establishment of *Picea abies* at around 8.2 ka[58,59]. *Picea* became a dominant component of the carr forest and likely expanded into nearby uplands forests. The reconstructed summer cooling is probably amplified by the local presence of *Picea abies* in Steregoiu, which tolerates very low summer temperatures (Fig. S3) and reached high pollen percentages (50–55%) at that time. The expansion of *Filipendula*, a taxon with also low temperature optima (Fig. S3), may further enhanced the cooling signal. Its increase reflects mire hydroseral development, and their affinity with boreal and temperate mire environments[60–62] suggests that local edaphic changes further distorted the regional climate signal, likely leading to an overestimation of the cooling amplitude.

Many other temperature records from ECE show either no clear expression of the event or only a weak signal[21]. One explanation could be that the cooling associated with the 8.2 ka event was strongest during winter and not well captured in proxies that primarily reflect summer conditions, such as chironomid-based temperature reconstructions. However, this interpretation could also be ruled out considering the cooling of 3.8 °C observed in the chironomid-based July temperature reconstruction from Hypkaňa[24].

Regarding possible changes in precipitation and/or humidity during 8.2 ka event, Warken et al. (2024) identified a pronounced climatic signal in their speleothem record, interpreting it as an increase in autumn-winter wetness (Fig. S6), consistent with the interpretation of Pál et al. (2016). In contrast, d-excess values from Scărișoara ice cave do not reflect dry-wet conditions or seasonality but changes in moisture sources. These data indicate that, during the 8.2 ka event, precipitation was derived from more evaporative and/or higher-evaporation regions[29], such as the eastern Mediterranean or the Black Sea[63,64]. Similarly, high $\delta^{13}C$ and Mg/Ca data from the Mituchovci tufa deposit in the northwestern Carpathians (S Slovakia) suggested dry conditions at 8.5 and 10.3 ka[65]. Together, these findings highlight inconsistencies among regional proxy records regarding precipitation changes during the 8.2 ka event. This underscores the need for additional high-resolution multiproxy studies integrated with climate model simulations to better constrain humidity conditions in the region.

No other statistically significant cold or warm excursions are detected in the ECE summer and winter temperature composites, suggesting that if additional Holocene rapid events occurred, their magnitudes were too small to be identified by the SnSiZer analysis. The strongest non-significant excursion is the cooling at 10.4–10.2 ka, during which both summer and winter reconstructions indicate a temperature decrease of 0.5 and 1.4 °C, respectively (Fig. 2). This suggested event may have been triggered by abrupt meltwater pulses from the Lakes Agassiz-Ojibway (Laurentide Ice Sheet) into the North Atlantic, which weakened the AMOC[66–68] and caused this cooling that affected our East-Central European region. However, this interpretation contrasts with the global proxy compilation of McKay et al. (2024), which does not identify a cold event at 10.3 ka, indicating that the cooling was neither sufficiently abrupt nor widespread to be clearly expressed at a global scale.

Conclusions

Our results demonstrate that Holocene temperature evolution in ECE was strongly seasonal. Summer temperatures increased rapidly by 1 °C during the Early Holocene (12–9.9 ka), reached a pronounced maximum between 9.5 and 5.5 ka with 1.1–2.4 °C warmer than present, and then declined gradually by 1.9 °C toward modern values, remaining relatively stable over the last 1.1 ka. In contrast, winter temperatures followed a different trajectory, with warming of 2.1 °C during the Early Holocene (12–9.2 ka)

continued to increase gradually by an additional 1.7 °C through the Mid and Late Holocene (7.8–2.6 ka). This warming culminated in a winter temperature maximum 2.1 ka ago, when values were 1.5 °C warmer than today, followed by a cooling of 0.7 °C between 1.7 and 0.4 ka. The opposing summer and winter temperature trends during the last 6 ka, and especially between 4.5 and 2 ka, indicate a Late Holocene reduction in continentality in ECE. The only statistically significant excursion of the Holocene occurred at 8.6–8.2 ka, associated with the 8.2 ka event and expressed as an abrupt summer and winter temperature decreases of 2 °C and 2.4 °C, respectively.

Our summer and winter temperature trends concur in broad terms with independent records based on speleothem $\delta^{18}O$ and chironomid data, thereby reinforcing the robustness and feasibility of our reconstructions. Moreover, the results are comparable with the Holocene trends in modelled summer and winter temperatures, ultimately driven by the seasonal insolation values. However, they deviate substantially from some of the earlier quantitative climate reconstructions based on pollen data from the same region and even from the same sites. This demonstrates the sensitivity of pollen-based climate reconstructions to the decisions with the selection of the calibration model and the fossil datasets used in the climate reconstructions. Ultimately, such decisions are always somewhat subjective and the reliability of the pollen-based reconstructions can be tested only by comparisons with records independent of pollen data.

Material and methods

Modern vegetation

The pollen records come from the hill belt and the lower montane belt, with the lowest altitude record located at 400 m and the highest altitude record at 1050 m. The hill belt (400–700 m) is characterized by a temperate climate, with mean annual temperatures of 6–7 °C and annual precipitation of 600–700 mm/yr[17]. Forests in this zone are dominated by mesothermophilous taxa such as *Carpinus betulus*, *Fagus sylvatica* and *Quercus* spp., forming associations including *Lathyro hallersteinii-Carpinetum* and *Carpino-Fagetum*. In the Southern Carpathians, thermophilous oak forests (*Quercetum frainetto-cerris*, *Quercetum petraeae-cerris*) are common. In the Northwestern Carpathians, *Tilia platyphyllos* and *Pinus sylvestris* play a more prominent role, forming *Tilio-Carpinetum* and *Pino-Quercetum* forest types[17,69].

The montane belt (700–1800 m) is characterized by a cooler climate, with mean annual temperatures of 2–6 °C and annual precipitation of 700–1100 mm/yr[17]. This zone supports the development of beech-dominated forests, either monospecific or mixed with spruce (*Picea abies*) and fir (*Abies alba*), as well as boreal spruce forests. It is divided into three sub-belts: the lower montane sub-belt (700–1100 m), dominated by pure beech forests develop on acidic brown soils, framed in the association *Symphyto cordati-Fagetum*, and *Festuco drymejae-Fagetum* communities; the middle montane sub-belt (1100–1350 m), comprising acidophilic beech mixed with fir, spruce and basophilic beech communities; and the upper montane sub-belt (1350–1800 m), characterized mainly by spruce forests on acidic soils with *Picea abies*, *Pinus cembra*, and *Larix decidua*, transitioning to subalpine *Pinus mugo* communities[17].

Importance of site selection

The selection of fossil records from the Carpathians was guided by several key factors. A central objective was to identify pollen records from sites where vegetation is particularly sensitive to both summer and winter temperature changes. To meet this requirement, one of the primary criteria in this study was the influence of altitude on vegetation dynamics, which led to a focus on mid-altitude sites. At these elevations, vegetation shows clear shifts in dominant tree species, largely driven by species-specific tolerances to temperature fluctuations[70]. Consequently, the mid-altitude Carpathians provide an optimal setting for reconstructing past temperature variability, with changes in forest composition reflecting the clear relationship between vegetation patterns and altitude-related temperature changes.

Taking these considerations into account, low-altitude sites below the hill belt (<400 m) were excluded to avoid environments characterized by excessively hot and dry summer conditions, where the distributions of key tree species such as *Quercus robur* and *Carpinus betulus* are primarily constrained by water availability rather than temperature[71–73]. These lowland settings are also more strongly influenced by human activity[74], further reducing their suitability for reconstructing temperature-driven vegetation dynamics. Substantial human impact on low-altitude vegetation have been documented in several records in this region, including Lake Balaton and Lake Kokad[37,75]. High-altitude records were also excluded because of the strong dominance of *Picea abies*, particularly above the upper montane sub-belt (>1350 m). Throughout the Holocene, fossil records from sites above this elevation, such as Poiana Ştiol (1550 m) and Gărgălău (1810 m), consistently show high abundances of *Picea abies* (20–60%)[40,76] and exhibit less pronounced vegetation changes than lower elevation sites. Consequently, the strong dominance of spruce may obscure the Holocene temperature variability, making high-altitude pollen records in this region less suitable for reconstructing past temperature changes.

Fossil pollen records

We focused on fossil pollen records from mid-altitude lakes and peat bogs within the hill belt and the lower and middle montane sub-belts (400–1350 m) of the Carpathian Mountains. In addition to the criterion of selecting mid-altitude records, we selected fossil pollen records with well-constrained chronological control, being the Avrig record the one with the fewest radiocarbon dates, with a total of six dates used in its age-depth model. In addition, the selected records must not show any evidence of abrupt changes in sediment accumulation rates. Due to limitations in site selection, we ultimately selected five fossil pollen records, which from north to south are: Hypkaňa peat bog (paleo-lake) (Slovakia, 48°54'48"N 22°09'49"E, 847 m a.s.l.)[24], Steregoiu rich fen (paleo-lake) (Romania, 47°48'48"N 23°32'41"E, 790 m a.s.l.)[20,58,59,77], Mohos peat bog (Romania, 46°08'03"N 25°54'18"E, 1049 m a.s.l.)[48,78], Sfânta Ana lake (Romania, 46°07'33"N 25°53'10"E, 946 m a.s.l.)[79–81] and Avrig peat bog (Romania, 45°42'50"N 24°23'37"E, 400 m a.s.l.)[49] (Fig. 1). These fossil pollen records were downloaded from the Neotoma database, and the age-depth models and calibration curves used are included in Table 1. The pollen diagrams for these records, including the main tree and herbaceous taxa, are represented in Figs. S7–S11. The composite abundances of the main tree pollen taxa from the five Carpathian fossil records spanning the last 12,000 years are shown in Fig. S1. The modern annual, summer and winter temperatures for each site were obtained from the WorldClim v2.1 data. For the selected records, temperatures range from 4.45 to 8.63 °C (annual), 13.63 to 18.5 °C (summer), and −5.26 to −1.83 °C (winter) (further details in Table 1).

Pollen-climate calibration model

The quantitative summer (June-July-August, JJA) and winter (December-January-February, DJF) temperature reconstructions of the Carpathian region were developed under the pollen-based transfer function approach, applying the Weighted Averaging-Partial Least Squares (WA-PLS) calibrated regression model. The approach is based on the principle that climate change significantly influences vegetation composition and distribution, as each plant species exhibits specific tolerances to temperature and humidity. The WA-PLS method uses the full calibration set to estimate relationships and, unlike other approaches (e.g., Modern Analogue Technique), it models continuous gradients in the dataset without requiring exact modern analogues. This makes it particularly suitable in cases where strong analogues are lacking, as it is the case of many paleo-records. Furthermore, this method assumes a unimodal relationship between individual taxa and climate variables and, compared to other approaches, is relatively robust to spatial autocorrelation[6].

The pollen-climate calibration model used for quantitative temperature reconstructions is based on pollen samples from the most recent version of the Eurasian Modern Pollen Database (EMPDv2)[82]. The use of the full EMPDv2 calibration set, together with the taxon harmonization procedure, leads to the combination of pollen types with distinct climatic niches. This can cause the variability of the harmonized taxa to reflect factors

Table 1 | Details of the fossil pollen sites used in this study

Site	Latitude	Longitude	Altitude	Type	Size (ha)	Country	Modern annual temperature (°C)	Modern summer temperature (°C)	Modern winter temperature (°C)	Modern annual precipitation (mm/yr)	Age-depth models and calibration curves
Hypkaňa	48°54'48"N	22°09'49"E	847	Lake	0.8	Slovakia	5.07	13.63	−3.78	1039	IntCal13 using Bacon (Hájková et al., 2016)
Steregoiu	47°48'48"N	23°32'41"E	790	Lake	0.5	Romania	5.08	13.65	−3.66	1120	Recalculated to IntCal09 (Neotoma)
Mohos	46°08'03"N	25°54'18"E	1049	Peat bog	80	Romania	4.45	13.86	−5.26	594	Recalculated to IntCal09 (Neotoma)
Sfânta Ana	46°07'33"N	25°53'10"E	946	Lake	19	Romania	4.71	14.21	−5.15	593	IntCal04 using Oxcal (Magyari et al., 2009)
Avrig	45°42'50"N	24°23'37"E	400	Peat bog	10	Romania	8.63	18.25	−1.83	625	Linear interpolation (Tanțău et al., 2006)

The modern climate parameters are based on WorldClim v2.1 data obtained for each site.

other than the climatic parameters selected for reconstruction, potentially reducing the accuracy of the paleoclimatic results. Therefore, instead of the full EMPDv2, we used a regionally-restricted subset of modern pollen samples from ECE for the seasonal temperature reconstruction. This calibration set is located between latitudes 42°N and 60°N and longitudes 13°E and 30°E, resulting in a total of 974 modern pollen samples (Fig. 1 and Table 2). The advantage of employing a regional calibration model is that the climatic gradients are comparatively simple, characterized by increasing summer and winter temperatures toward the south. Moreover, the taxonomic harmonization at regional scale ensures that most major taxa are represented by a single or few dominant species. In ECE, dominant tree species include *Fagus sylvatica* (represented by *Fagus* pollen type), *Carpinus betulus* and *C. orientalis* (represented by *Carpinus* pollen type), *Quercus robur*, *Q. cerris*, *Q. pubescens* and *Q. petraea* (represented by *Quercus* pollen type), *Corylus avellana* (represented by *Corylus* pollen type), *Fraxinus excelsior* and *F. angustifolia* (represented by *Fraxinus* pollen type), *Ulmus glabra* and *U. minor* (represented by *Ulmus* pollen type), *Betula pendula* and *B. pubescens* (represented by *Betula* pollen type), *Picea abies* (represented by *Picea* pollen type), and *Pinus mugo*, *P. sylvestris* and *P. cembra* (represented by *Pinus* pollen type). Because most common pollen types correspond to one or two tree species, the resulting estimates of pollen-type optima and tolerances are more precise than those derived from continental-scale datasets.

The taxonomic harmonization of pollen data was developed on the EMPDv2 and the fossil pollen records. Minor taxa and those with low relative abundances were merged into broader taxonomic groups at the genus or family level, which resulted in a total of 256 harmonized taxa. This process was done using the Plants of the World Online database (https://powo.science.kew.org) and the Integrated Taxonomic Information System (https://www.itis.gov). Aquatics (i.e., *Callitriche*, *Caltha*, Cyperaceae, Juncaceae, *Lemna*, Lythraceae, *Lythrum*, *Myriophyllum*, *Nuphar*, *Phragmites*), non-native (i.e., *Eucalyptus*), cultivated plants (i.e., *Avena*, *Zea mays*) and pollen of plants with local signal (i.e., *Erica*, Ericaceae, *Vaccinium*) were excluded because their presence could be influenced by non-climate related factors (in the case of aquatic and local plants) or generate wrong quantitative results for the study region (in the case of non-native plants). Table S1 provides additional information on the species identified in the original pollen studies for each record, which we have grouped into broader taxonomic categories to perform the reconstructions. The modern summer and winter temperature data were obtained from the WorldClim v2.1 database at a 30-second resolution (www.worldclim.org).

Model performance statistics

We used the two-component WA-PLS model because increasing the number of components can lead to overfitting of the data, which in turn decreases the predictive value of the model[83]. To reduce noise in the data, a square-root transformation was applied to species abundances in the modern pollen calibration set. The performance of the WA-PLS regression model was assessed using the leave-one-out cross-validation approach[84]. From the cross-validation results, we calculated key performance metrics, including the coefficient of determination (R^2), the root mean square error of prediction (RMSEP) and the maximum bias. The performance statistics for the summer temperature statistics provided a R^2 of 0.52, an average bias of 0.06 °C, maximum bias of 8.91 °C and RMSEP of 1.38 °C, whereas the winter temperature reported a R^2 of 0.55, an average bias of 0.05 °C, maximum bias of 10.46 °C and RMSEP of 1.30 °C (Table 2 and Fig. S12). The reconstructions were conducted using the C2 software (version 1.8.0)[85].

The positive residual values, specifically for the lowest observed temperatures (Fig. S12), suggest that the coldest reconstructed summer and winter temperatures could have been overestimated for values below ca. 11 °C in summer and −6 °C in winter. Since the reconstructed temperatures for each record are several degrees higher than these values, it is unlikely that the reconstructions have been affected by these modern pollen samples from cold regions, and therefore that they have influenced the results.

Table 2 | Detailed information of the pollen-climate calibration model used and the performance statistics

Pollen-climate calibration model							
Modern pollen database	**Modern climate parameters**	**Calibration set**	**Raw summer temperature gradient**		**Raw winter temperature gradient**	**Modern pollen samples**	**Harmonized taxa**
EMPDv2	WorldClim v2.1 (30-sec res.)	East-Central Europe (ECE) (Lat 42–60°N, Log 13–30°E)	Max: 24.23 °C Min: 7.80 °C		Max: 7.97 °C Min: −7.70 °C	974	256
Model performance statistics							
Climate parameter		**Component**	R^2	**Aver. Bias**	**Max. Bias**		**RMSEP**
Temperature JJA		1	0.389	0.036	6.573		1.563
Temperature JJA		**2**	**0.518**	**0.067**	**8.910**		**1.385**
Temperature JJA		3	0.580	0.029	10.260		1.294
Temperature JJA		4	0.573	0.024	11.593		1.309
Temperature JJA		5	0.557	0.029	13.011		1.344
Temperature DJF		1	0.474	0.047	8.787		1.416
Temperature DJF		**2**	**0.553**	**0.050**	**10.460**		**1.306**
Temperature DJF		3	0.593	0.024	10.620		1.247
Temperature DJF		4	0.589	0.019	11.470		1.260
Temperature DJF		5	0.571	0.030	11.460		1.296

In addition, we performed the RandomTF analysis[86] to evaluate whether quantitative temperature reconstructions based on the fossil records are statistically significant and how much of the variation in the fossil data is explained by summer and winter temperatures. In this study, 999 random transfer functions were generated, revealing that six out of a total of ten reconstructions (summer and winter in each of the five records) are statistically significant ($p < 0.1$) and outperform 90% of random reconstructions, indicating that these reconstructions explained much more variance than the 999 random reconstructions (Fig. S13). In contrast, two summer temperatures at low-altitude sites and two winter temperatures at high altitudes can be considered not significant ($p > 0.1$) (Figs. S13 and S14), suggesting that summer temperatures may be more variable at lower elevations, whereas winter temperatures show greater variability at higher elevations. This does not mean that the reconstructions are incorrect, but rather that the fossil vegetation data from summer at low elevations and winter at high elevations may also be influenced by other climatic parameters.

Individual time-series climate records are typically noisy and contain chronological uncertainties. To more reliably identify Holocene seasonal temperature patterns that reflect the regional climate signal of the Carpathians, and, given that the pollen records originate from similar ecological zones and display comparable Holocene vegetation dynamics, the individual summer and winter temperature reconstructions from the five fossil pollen records were combined to produce two composite temperature curves. These composite curves were generated by first calculating, for each fossil sample, the temperature anomaly relative to the Holocene mean within each record. The temperature deviation data from all five sites were then merged into a single dataset, ordered from the youngest to the oldest sample, containing both sample age and the corresponding temperature anomaly. The resulting summer and winter temperature composites consist of 736 samples for the last 12 ka. This enables the detection of short-term temperature variability and strengthens the robustness of the paleoclimatic interpretations. To better visualize both short- and long-term temperature changes throughout the Holocene, a LOESS smoothing parameter of 0.015 was applied to the two composite curves.

In addition, 100-yr bins were generated based on the lowest-resolution record Sfânta Ana. Although binning reduces the temporal resolution of the summer and winter temperature records, it provides a useful cross-check to identify and remove any potential spurious patterns in the dataset. Consequently, such artefacts would become evident when comparing the composite record with the same record resampled at uniform 100-year intervals.

SnSiZer analysis—identification of statistically significant changes in temperature reconstructions

Quantitative climate reconstruction based on biological proxies are inherently noisy and wiggly and it is therefore important to statistically assess the significance of the evidence of excursions in the datasets[4,9,10]. Here we use SnSizer. Both the original SiZer method[87] and the more recent SnSiZer use nonparametric smoothing to identify intervals of statistically significant increasing or decreasing trends in the data. SnSiZer extends the functionality of SiZer by applying multiple levels of smoothing, thereby revealing key features across different temporal scales.

The results of SnSiZer analysis are typically visualized on a two-dimensional plot, with time on the horizontal axis and the logarithm of the smoothing parameter $\log_{10}(h)$ on the vertical axis, representing different levels of smoothing. The color scheme indicates the statistical significance of the first derivative of the smoothed signal at each time point and smoothing level: red regions indicate statistically significant positive trends (increasing temperatures), blue regions indicate significant negative trends (decreasing temperatures), dark gray indicates non-significant trends, and light gray highlights areas where the data resolution is insufficient to detect changes with confidence. Superimposed on this color plot are smoothed time series curves representing different levels of smoothing, including green (lowest smoothing level) and yellow (intermediate smoothing level) curves for the short-term temperature trends, and orange (highest smoothing level) for the

long-term trends. These curves help to visually identify where the signal intersects regions of statistically significant trends. When one of these curves intersects a red or blue region, it indicates that the trend at that smoothing level is statistically significant.

To assess the relative strength of increases and decreases, the color intensity reflects the magnitude of the first derivative of the smoothed signal. However, since smoothing reduces the magnitude of the derivatives, it is not possible to make direct comparisons between the intensity of the increases and decreases at different smoothing levels. To address this, normalized scale-space derivatives can be employed[88]. These derivatives are scaled relative to the smoothing level, making them appropriate for comparing features across multiple scales and identifying characteristic patterns within time series data. The SnSiZer analysis was implemented in RStudio (version 2024.09.0; www.rstudio.com) through modifications to the source code of the original SiZer package. The original code of the SiZer package (version 0.1–8) can be found in the GitHub repository (https://github.com/dereksonderegger/SiZer)[89].

The SnSiZer results have been classified into trends and excursions. Trends refer to statistically significant long-term temperature changes (orange smoothing level), whereas the excursions show the statistically significant short-term temperature changes (yellow and green smoothing levels) identified in this analysis (Figs. 3 and 4). For ease of reading, we use "ka" instead of "cal ka BP" throughout the text.

Reporting summary

Further information on research design is available in the Nature Portfolio Reporting Summary linked to this article.

Data availability

The mean summer and winter temperature deviations (°C) from the Holocene mean for East-Central Europe, derived from Carpathian fossil pollen records, are available in Figshare data repository via the following link: https://doi.org/10.6084/m9.figshare.31970106.

Received: 9 April 2026; Accepted: 27 August 2026;
Published online: 14 September 2026

References

1. Bova, S., Rosenthal, Y., Liu, Z., Godad, S. P. & Yan, M. Seasonal origin of the thermal maxima at the Holocene and the last interglacial. *Nature* **589**, 548–553 (2021).
2. Holtzman, H. et al. Early Holocene atmospheric circulation changes over northern Europe based on isotopic and biomarker evidence from Kola Peninsula. *Paleoceanogr. Paleoclimatol.* **40**, e2024PA005076 (2025).
3. Kaufman, D. S. & Broadman, E. Revisiting the Holocene global temperature conundrum. *Nature* **614**, 425–435 (2023).
4. Fletcher, W. J., Sánchez Goñi, M. F., Naughton, F. & Seppä, H. in *European Glacial Landscapes* (eds Palacios, D. et al.) 127–146 (Elsevier, 2024).
5. Seppä, H., Birks, H. J. B., Odland, A., Poska, A. & Veski, S. A modern pollen–climate calibration set from northern Europe: developing and testing a tool for palaeoclimatological reconstructions. *J. Biogeogr.* **31**, 251–267 (2004).
6. Telford, R. J. & Birks, H. J. B. The secret assumption of transfer functions: problems with spatial autocorrelation in evaluating model performance. *Quat. Sci. Rev.* **24**, 2173–2179 (2005).
7. Birks, H. J. B., Heiri, O., Seppä, H. & Bjune, A. E. J. Strengths and weaknesses of quantitative climate reconstructions based on Late-Quaternary biological proxies. *Open Ecol. J.* **3**, 68–110 (2010).
8. Samartin, S. et al. Warm Mediterranean mid-Holocene summers inferred from fossil midge assemblages. *Nat. Geosci.* **10**, 207–212 (2017).
9. Morrill, C. et al. Proxy benchmarks for intercomparison of 8.2 ka simulations. *Climate Past* **9**, 423–432 (2013).
10. McKay, N. P. et al. The 4.2 ka event is not remarkable in the context of Holocene climate variability. *Nat. Commun.* **15**, 6555 (2024).
11. Camuera, J. et al. Occurrence of Heinrich stadials in the West Mediterranean and West African regions and their connections to atmospheric circulation changes. *Commun. Earth Environ.* **7**, 94 (2026).
12. Liu, Z. et al. The Holocene temperature conundrum. *Proc. Natl. Acad. Sci. USA* **111**, E3501–E3505 (2014).
13. Kaufman, D. et al. A global database of Holocene paleotemperature records. *Sci. Data* **7**, 115 (2020).
14. Huntley, B. Reconstructing palaeoclimates from biological proxies: some often overlooked sources of uncertainty. *Quat. Sci. Rev.* **31**, 1–16 (2012).
15. Chevalier, M. et al. Pollen-based climate reconstruction techniques for late Quaternary studies. *Earth-Sci. Rev.* **210**, 103384 (2020).
16. Crawford, R. M. *Plants at the Margin: Ecological Limits and Climate Change* (Cambridge University Press, 2008).
17. Coldea, G. & Cristea, V. Syntaxonomic characterization of the vegetation belts from the South-eastern Carpathians (Romanian Carpathians). *Flora Mediterr.* **31**, 361–369 (2021).
18. Jovanović, I., Dragišić, A., Ostojić, D. & Krsteski, B. J. F. Beech forests as world heritage in aspect to the next extension of the ancient and primeval beech forests of the Carpathians and other regions of Europe world heritage site. *Zaštita Prir.* **69**, 15–32 (2019).
19. Sabatini, F. M. et al. Where are Europe's last primary forests?. *Divers. Distrib.* **24**, 1426–1439 (2018).
20. Feurdean, A., Klotz, S., Mosbrugger, V. & Wohlfarth, B. Pollen-based quantitative reconstructions of Holocene climate variability in NW Romania. *Palaeogeogr. Palaeoclimatol. Palaeogeogr.* **260**, 494–504 (2008).
21. Tóth, M. et al. Chironomid-inferred Holocene temperature changes in the South Carpathians (Romania). *Holocene* **25**, 569–582 (2015).
22. Formáčková, A. et al. Holocene summer temperature variability in the Southern Carpathians: possible North Atlantic Jet forcing and high-altitude sensitivity. *Quat. Sci. Rev.* **360**, 109378 (2025).
23. Szabó, Z. et al. Two chironomid-inferred mean July air temperature reconstructions in the South Carpathian Mountains over the last 2000 years. *Holocene* **34**, 987–1004 (2024).
24. Hájková, P. et al. A first chironomid-based summer temperature reconstruction (13–5 ka BP) around 49°N in inland Europe compared with local lake development. *Quat. Sci. Rev.* **141**, 94–111 (2016).
25. Buczkó, K., Szurdoki, E., Braun, M. & Magyari, E. Reconciling diverse diatom-based lake responses to climate change in four mountain lakes in the South-Carpathian Mountains during the last 17 kyrs. *Quat. Int.* **477**, 117–137 (2018).
26. Büntgen, U. et al. Filling the Eastern European gap in millennium-long temperature reconstructions. *Proc. Natl. Acad. Sci. USA* **110**, 1773–1778 (2013).
27. Nagavciuc, V., Ionita, M., Kern, Z., McCarroll, D. & Popa, I. A ~700 years perspective on the 21st century drying in the eastern part of Europe based on δ18O in tree ring cellulose. *Commun. Earth Environ.* **3**, 277 (2022).
28. Ramos-Román, M. J. et al. Lipid biomarker (brGDGT)- and pollen-based reconstruction of temperature change during the Middle to Late Holocene transition in the Carpathians. *Glob. Planet. Change* **215**, 103859 (2022).
29. Perşoiu, A. et al. Holocene winter climate variability in Central and Eastern Europe. *Sci. Rep.* **7**, 1196 (2017).
30. Haliuc, A. et al. Palaeohydrological changes during the mid and late Holocene in the Carpathian area, central-eastern Europe. *Glob. Planet. Change* **152**, 99–114 (2017).
31. Longman, J., Veres, D., Ersek, V., Haliuc, A. & Wennrich, V. Runoff events and related rainfall variability in the Southern Carpathians during the last 2000 years. *Sci. Rep.* **9**, 5334 (2019).

32. Diaconu, A.-C. et al. A multi-proxy analysis of hydroclimate trends in an ombrotrophic bog over the last millennium in the Eastern Carpathians of Romania. *Palaeogeogr., Palaeoclimatol., Palaeoecol.* **538**, 109390 (2020).
33. Ruskál, A., Diaconu, A.-C., Grindean, R. & Tanțău, I. Early to mid-Holocene hydroclimate trends in the western Carpathians of Romania. *Palaeogeogr. Palaeoclimatol. Palaeoecol.* **543**, 109608 (2020).
34. Micu, D. M., Dumitrescu, A., Cheval, S., Nita, I.-A. & Birsan, M.-V. Temperature changes and elevation-warming relationships in the Carpathian Mountains. *Int. J. Climatol.* **41**, 2154–2172 (2021).
35. Gumnior, M. & Stobbe, A. First palynological results from lowland sites in the Romanian Banat and their implications for settlement and land use dynamics in the southeastern Carpathian Basin. *Quat. Int.* **583**, 48–61 (2021).
36. Magyari, E. K. et al. Review on vegetation, landscape and climate changes in the Carpathian Basin during the Neolithic and Chalcolithic period. *Veg. Hist. Archaeobotany* **33**, 769–794 (2024).
37. Pál, I. et al. Holocene land cover change in the Pannonian (East-Central Europe) forest steppe: the role of prehistoric land exploitation phases. *Quat. Environ. Hum.* **3**, 100077 (2025).
38. Finsinger, W. et al. Holocene fire-regime changes near the treeline in the Retezat Mts. (Southern Carpathians, Romania). *Quat. Int.* **477**, 94–105 (2018).
39. Wiezik, M. et al. Transformation of West-Carpathian primeval woodlands into high-altitude grasslands from as early as the Bronze Age. *Veg. Hist. Archaeobotany* **32**, 205–220 (2023).
40. Feurdean, A. et al. Tree and timberline shifts in the northern Romanian Carpathians during the Holocene and the responses to environmental changes. *Quat. Sci. Rev.* **134**, 100–113 (2016).
41. Árvai, M., Popa, I., Mîndrescu, M., Nagy, B. & Kern, Z. Dendrochronology and radiocarbon dating of subfossil conifer logs from a peat bog, Maramureş Mts, Romania. *Quat. Int.* **415**, 6–14 (2016).
42. Broström, A. et al. Pollen productivity estimates of key European plant taxa for quantitative reconstruction of past vegetation: a review. *Veg. Hist. Archaeobotany* **17**, 461–478 (2008).
43. Feurdean, A. et al. Fire has been an important driver of forest dynamics in the Carpathian Mountains during the Holocene. *For. Ecol. Manag.* **389**, 15–26 (2017).
44. Sykes, M. T., Prentice, I. C. & Cramer, W. A bioclimatic model for the potential distributions of north European tree species under present and future climates. *J. Biogeogr.* **23**, 203–233 (1996).
45. Finsinger, W., Tinner, W., van der Knaap, W. O. & Ammann, B. The expansion of hazel (Corylus avellana L.) in the southern Alps: a key for understanding its early Holocene history in Europe? *Quat. Sci. Rev.* **25**, 612–631 (2006).
46. Theuerkauf, M. et al. Corylus expansion and persistent openness in the early Holocene vegetation of northern central Europe. *Quat. Sci. Rev.* **90**, 183–198 (2014).
47. Mogîldea, D., Sahlean, T. C. & Biță-Nicolae, C. Riparian forests of alnus species communities and their role in sustainability in the Romanian Carpathians and adjacent regions. *Sustainability* **16**, 4130 (2024).
48. Tanțău, I., Grindean, R. & Magyari, E. K. in *Ciomadul (Csomád), The Youngest Volcano in the Carpathians: Volcanism, Palaeoenvironment, Human Impact* (eds Karátson, D. et al.) 175–185 (Springer International Publishing, 2022).
49. Tanțău, I., Reille, M., de Beaulieu, J.-L. & Farcas, S. Late Glacial and Holocene vegetation history in the southern part of Transylvania (Romania): pollen analysis of two sequences from Avrig. *J. Quat. Sci.* **21**, 49–61 (2006).
50. Cruz-Silva, E. et al. Pollen-based reconstructions of Holocene climate trends in the eastern Mediterranean region. *Climate Past* **19**, 2093–2108 (2023).
51. Karger, D. N., Nobis, M. P., Normand, S., Graham, C. H. & Zimmermann, N. E. CHELSA-TraCE21k – high-resolution (1 km) downscaled transient temperature and precipitation data since the Last Glacial Maximum. *Climate Past* **19**, 439–456 (2023).
52. Liu, Z. et al. Transient simulation of last deglaciation with a new mechanism for Bølling-Allerød warming. *Science* **325**, 310–314 (2009).
53. Drăguşin, V., Ersek, V., Fleitmann, D., Ionita, M. & Onac, B. P. Winter hydroclimate contrasts between southern and northern Europe at ~ 5.2 ka. *Palaeogeogr. Palaeoclimatol. Palaeoecol.* **632**, 111863 (2023).
54. Alley, R. B. et al. Holocene climatic instability: a prominent, widespread event 8200 yr ago. *Geology* **25**, 483–486 (1997).
55. Rohling, E. J. & Pälike, H. Centennial-scale climate cooling with a sudden cold event around 8,200 years ago. *Nature* **434**, 975–979 (2005).
56. Hoffman, J. S. et al. Linking the 8.2 ka event and its freshwater forcing in the Labrador Sea. *Geophys. Res. Lett.* **39**, L18703 (2012).
57. Matero, I. S. O., Gregoire, L. J., Ivanovic, R. F., Tindall, J. C. & Haywood, A. M. The 8.2 ka cooling event caused by Laurentide ice saddle collapse. *Earth Planet. Sci. Lett.* **473**, 205–214 (2017).
58. Feurdean, A. & Bennike, O. Late Quaternary palaeoecological and palaeoclimatological reconstruction in the Gutaiului Mountains, northwest Romania. *J. Quat. Sci.* **19**, 809–827 (2004).
59. Björkman, L., Feurdean, A. & Wohlfarth, B. Late-Glacial and Holocene forest dynamics at Steregoiu in the Gutaiului Mountains, Northwest Romania. *Rev. Palaeobot. Palynol.* **124**, 79–111 (2003).
60. Smirnova, O. V., Kalyakin, V. N., Turubanova, S. A., Bobrovsky, M. V. & Khanina, L. G. in *European Russian Forests: Their Current State and Features of their History* (eds Smirnova, O. V. et al.) 515–536 (Springer Netherlands, 2017).
61. Warken, S. F. et al. Dynamic processes determine precipitation variability in Eastern Central Europe since the Last Glacial Maximum. *Commun. Earth Environ.* **5**, 694 (2024).
62. Pál, I. et al. Small-scale moisture availability increase during the 8.2-ka climatic event inferred from biotic proxy records in the South Carpathians (SE Romania). *Holocene* **26**, 1382–1396 (2016).
63. Perşoiu, A., Ionita, M. & Weiss, H. Atmospheric blocking induced by the strengthened Siberian High led to drying in west Asia during the 4.2 ka BP event – a hypothesis. *Climate Past* **15**, 781–793 (2019).
64. Demény, A. et al. A speleothem record of seasonality and moisture transport around the 8.2 ka event in Central Europe (Vacska Cave, Hungary). *Quat. Res.* **118**, 195–210 (2024).
65. Dabkowski, J. et al. A complete Holocene climate and environment record for the Western Carpathians (Slovakia) derived from a tufa deposit. *Holocene* **29**, 493–504 (2019).
66. Clark, P. U. et al. Freshwater forcing of abrupt climate change during the last glaciation. *Science* **293**, 283–287 (2001).
67. Fisher, T. G., Smith, D. G. & Andrews, J. T. Preboreal oscillation caused by a glacial Lake Agassiz flood. *Quat. Sci. Rev.* **21**, 873–878 (2002).
68. Teller, J. T., Leverington, D. W. & Mann, J. D. Freshwater outbursts to the oceans from glacial Lake Agassiz and their role in climate change during the last deglaciation. *Quat. Sci. Rev.* **21**, 879–887 (2002).
69. Zarzycki, K. 109–121 (Stiftung Rübel, 1991).
70. Feurdean, A., Tămaş, T., Tanțău, I. & Fărcaş, S. Elevational variation in regional vegetation responses to late-glacial climate changes in the Carpathians. *J. Biogeogr.* **39**, 258–271 (2012).
71. Bede-Fazekas, Á, Török, P. & Erdős, L. Empirical delineation of the forest-steppe zone is supported by macroclimate. *Sci. Rep.* **13**, 17379 (2023).
72. Erdős, L. et al. Oak regeneration at the arid boundary of the temperate deciduous forest biome: insights from a seeding and watering experiment. *Eur. J. For. Res.* **140**, 589–601 (2021).

73. Tölgyesi, C. et al. Underground deserts below fertility islands? Woody species desiccate lower soil layers in sandy drylands. *Ecography* **43**, 848–859 (2020).
74. Szatmari, P.-M. & Hurdu, B.-I. Low altitude glacial relicts in the Romanian flora. *Contrib. Bot.* **57**, 19–51 (2022).
75. Sümegi, P., Persaits, G. & Gulyás, S. in *Ecotones Between Forest and Grassland* (eds Myster, R. W.) 17–57 (Springer New York, 2012).
76. Tanțău, I. et al. Holocene vegetation history in the upper forest belt of the Eastern Romanian Carpathians. *Palaeogeogr. Palaeoclimatol. Palaeoecol.* **309**, 281–290 (2011).
77. Björkman, L., Feurdean, A., Cinthio, K., Wohlfarth, B. & Possnert, G. Lateglacial and early Holocene vegetation development in the Gutaiului Mountains, northwestern Romania. *Quat. Sci. Rev.* **21**, 1039–1059 (2002).
78. Tanțău, I. et al. Vegetation history in the Eastern Romanian Carpathians: pollen analysis of two sequences from the Mohoş crater. *Veg. Hist. Archaeobotany* **12**, 113–125 (2003).
79. Magyari, E. et al. Palaeolimnology of the last crater lake in the Eastern Carpathian Mountains: a multiproxy study of Holocene hydrological changes. *Hydrobiologia* **631**, 29–63 (2009).
80. Magyari, E. et al. Holocene palaeohydrology and environmental history in the South Harghita Mountains, Romania. *Földt. Közl.* **136**, 249–284 (2006).
81. Magyari, E. K. et al. in *Ciomadul (Csomád), The Youngest Volcano in the Carpathians: Volcanism, Palaeoenvironment, Human Impact* (eds Karátson, D. et al.) 145–158 (Springer International Publishing, 2022).
82. Davis, B. A. S. et al. The Eurasian Modern Pollen Database (EMPD), version 2. *Earth Syst. Sci. Data* **12**, 2423–2445 (2020).
83. Ter Braak, C., Juggins, S., Birks, H. & Van der Voet, H. in *Multivariate environmental statistics* (eds Patil, G. P. & Rao, C. R.) 525–560 (Elsevier, 1993).
84. Birks, H. J. B. et al. Diatoms and pH reconstruction. *Philos. Trans. R. Soc. Lond. B* **327**, 263–278 (1990).
85. Juggins, S. 73 (Newcastle upon Tyne, Newcastle University, UK, 2007).
86. Telford, R. J. & Birks, H. J. B. A novel method for assessing the statistical significance of quantitative reconstructions inferred from biotic assemblages. *Quat. Sci. Rev.* **30**, 1272–1278 (2011).
87. Chaudhuri, P. & Marron, J. S. SiZer for exploration of structures in curves. *J. Am. Stat. Assoc.* **94**, 807–823 (1999).
88. Lindeberg, T. Feature detection with automatic scale selection. *Int. J. Comput. Vis.* **30**, 79–116 (1998).
89. Sonderegger, D. L., Wang, H., Clements, W. H. & Noon, B. R. Using SiZer to detect thresholds in ecological data. *Front. Ecol. Environ.* **7**, 190–195 (2009).
90. Laskar, J. et al. A long-term numerical solution for the insolation quantities of the Earth. *Astron. Astrophys.* **428**, 261–285 (2004).

Acknowledgements

We gratefully acknowledge all researchers who have contributed modern pollen data to the Eurasian Modern Pollen Database and those who have made fossil pollen records accessible through open databases, thereby supporting reproducible and collaborative paleoclimate research.

Author contributions

J.C., E.K.M., and H.S. conceptualized the study, compiled the raw pollen data and prepared the initial manuscript draft. J.C. developed the quantitative reconstructions and performed the SnSiZer analyses, and J.L.K. help with the statistical analyses. Y.X., J.C., and H.S. obtained the model simulation data. J.L.K., N.K., L.C., A.A.O.-B., and Y.X. contributed to the interpretation of the results and discussion. All authors participated in writing and refining the manuscript.

Funding

This work was supported by project ERC-2017-ADG-788616 (YMPACT) funded by the European Commission/H2020 and the “Frontline” Research Excellence Programme no. 144209: The Domino Effect: Tracking changes in climate, environment and subsistence economy at the collapse of Neolithic lifestyle in Eastern-Central and South-East Europe (DOMINO- CLIMATE). This work has been also implemented by the National Multidisciplinary Laboratory for Climate Change (RRF-2.3.1-21-2022-00014) project within the framework of Hungary’s National Recovery and Resilience Plan supported by the Recovery and Resilience Facility of the European Union. J.C. also acknowledges the postdoctoral contract DGP_POST_2024_00267 funded by the Junta de Andalucía.

Competing interests

The authors declare no competing interests.

Additional information

Supplementary information The online version contains supplementary material available at https://doi.org/10.1038/s43247-026-04041-6.

Correspondence and requests for materials should be addressed to Jon Camuera or Enikő K. Magyari.

Reprints and permissions information is available at http://www.nature.com/reprints

Publisher’s note Springer Nature remains neutral with regard to jurisdictional claims in published maps and institutional affiliations.

Open Access This article is licensed under a Creative Commons Attribution-NonCommercial-NoDerivatives 4.0 International License, which permits any non-commercial use, sharing, distribution and reproduction in any medium or format, as long as you give appropriate credit to the original author(s) and the source, provide a link to the Creative Commons licence, and indicate if you modified the licensed material. You do not have permission under this licence to share adapted material derived from this article or parts of it. The images or other third party material in this article are included in the article's Creative Commons licence, unless indicated otherwise in a credit line to the material. If material is not included in the article's Creative Commons licence and your intended use is not permitted by statutory regulation or exceeds the permitted use, you will need to obtain permission directly from the copyright holder. To view a copy of this licence, visit http://creativecommons.org/licenses/by-nc-nd/4.0/.

© The Author(s) 2026

This Article in Press is shared early to give you faster access to new research. It is citable and carries a permanent DOI. The final edited version will replace it automatically.